Food Bioscience 68 (2025) 106496

Contents lists available at ScienceDirect

Food Bioscience

journal homepage: www.elsevier.com/locate/fbio

Comparative analysis of muscle quality, transcriptomic, and metabolomic profiles in yellow-mutant and wild-type northern snakehead (*Channa argus*): Implications for food quality and aquaculture breeding potential

Donglei Sun [a], Zexin Tao [a], Haishen Wen [a], Xin Qi [a], Chao Li [b], Lingyu Wang [a], Xiaoyan Zhang [b], Yun Li [a,*]

[a] Key Laboratory of Mariculture (Ocean University of China), Ministry of Education (KLMME), Fisheries College, Ocean University of China, Qingdao, 266003, China
[b] School of Marine Science and Engineering, Qingdao Agricultural University, Qingdao, 266109, China

ARTICLE INFO

Keywords:
Northern snakehead
Yellow-mutant strain
Muscle quality
Transcriptome
Metabolome

ABSTRACT

Northern snakehead (*Channa argus*) is an important freshwater fish species in China, with a recently discovered yellow-mutant (YM) strain. The YM snakehead holds significant potential for selective breeding and commercial value due to its superior appearance. However, its muscle quality differences compared to the wild-type (WT) strain remain unclear. This study compared flesh quality traits between YM and WT snakeheads and applied integrated transcriptomic and metabolomic analyses to uncover underlying molecular mechanisms.The flesh quality measurement results revealed that YM snakehead exhibited significantly higher muscle redness and n-3 PUFA content, particularly DHA, along with a significantly lower fishy odor compared to WT. Metabolomic profiling identified 42 differential metabolites (DMs), including DHA, IMP, and glycerophosphocholine related to lipid metabolism, and nicotinamide, trigonelline, and glutathione involved in redox processes. Transcriptomic analysis revealed 380 differentially expressed genes (DEGs), enriched in pathways oxidative phosphorylation (e.g., *myh13*, *atp5f1e*) and lipid metabolism (e.g., *pnpla7*, *lipe*). Integrated omics analysis suggested that lipid metabolism related DEGs and DMs may modulate nutritional value and flavor via the "Glycerophospholipid metabolism" pathway, while redox related metabolites and genes may influence muscle color by modulating myoglobin accumulation via the "Nicotinate and nicotinamide metabolism" pathway. These findings not only provide evidence supporting the superior flesh quality of the YM strain over the wild type and elucidate the molecular mechanisms underlying flesh quality differences between the two strains, but also offer a theoretical foundation for evaluating the economic potential of YM snakehead and guiding future breeding programs in aquaculture.

1. Introduction

Northern snakehead, *Channa argus* (Perciformes: Channidae), is a freshwater species of significant economic importance in East Asian aquaculture (Wang & Yang, 2011). The snakehead has emerged as an important breeding species of Chinese aquaculture, yielding an annual production exceeding 500,000 tons, driven by its exceptional growth performance, superior nutritional profile, and remarkable environmental resilience (Sun et al., 2023). In contrast to the wild-type (WT) phenotype characterized by grayish-black pigmentation, a yellow-mutant (YM) strain originating from Shandong Province, China, displays distinct golden-yellow coloration, red eyes, and reddish muscle. Critically, YM strain exhibit non-inferior growth performance compared to WT snakehead while demonstrating substantial market premiums in both food and ornamental aquaculture sectors. This dual-market superiority, driven by enhanced consumer preference and premium pricing, positions the YM strain as a novel aquaculture candidate capable of elevating economic sustainability in commercial breeding industry. While our prior work elucidated the *slc45a2* gene mutation underlying YM pigmentation (Sun et al., 2023), the differences in flesh quality between YM and WT snakeheads have not been thoroughly investigated. Specifically, the biochemical and organoleptic properties that determine flesh quality and the regulatory relationships underlying their gene expression have not been systematically studied.

* Corresponding author.
E-mail address: yunli0116@ouc.edu.cn (Y. Li).

https://doi.org/10.1016/j.fbio.2025.106496
Received 11 December 2024; Received in revised form 26 March 2025; Accepted 31 March 2025
Available online 1 April 2025

Muscle tissue, constituting the principal edible portion of fish, significantly influences consumer preferences and thus plays a crucial role in the commercial value of fish. Key organoleptic parameters governing flesh quality encompass textural properties, chromatic characteristics, biochemical composition, and flavor profiles (Fauconneau et al., 1995; Hayat et al., 2024; Ling et al., 2023). These quality attributes are modulated through complex interactions between environmental factors (e.g., farming conditions, nutritional supply) and genetic determinants (Beg et al., 2023; Khan et al., 2023; Zhao, Chong, et al., 2018), with flesh quality optimization representing a central objective in modern selective breeding programs (Gjedrem, 1997). The systematic characterization of flesh quality disparities between YM and WT snakeheads therefore holds substantial implications for advancing precision breeding strategies in snakehead aquaculture.

Metabolomics enables comprehensive characterization of low-molecular-weight metabolites within biological systems through advanced analytical platforms (Beyoğlu & Idle, 2013; Fiehn, 2002). While gas chromatography-mass spectrometry (GC-MS) remains widely utilized, liquid chromatography-mass spectrometry (LC-MS) has emerged as the gold standard due to its superior sensitivity, enhanced coverage of thermolabile compounds, and capacity to resolve high molecular weight metabolites (Zhou et al., 2012). Given that muscle metabolites significantly influence nutrition, flavor, and degradation processes, Metabolomics enables more fine-grained evaluation of muscle quality differences (Young & Alfaro, 2018). Previous studies have effectively employed metabolomics in fish muscle tissue research, such as examining flesh quality differentiation in grass carp (*Ctenopharyngodon idella*) based on diet (Zhao, Chong, et al., 2018) and comparing the metabolic profiles of tuna muscle across species and geographic regions (Bodin et al., 2022).

Recent advances in multi-omics technologies have revolutionized the mechanistic understanding of muscle quality in aquatic species, offering unprecedented resolution to decode the complex interplay between transcriptional regulation and metabolic dynamics. Conventional single-omics approaches, while informative, often fail to capture the systemic interactions driving phenotypic variations in texture, flavor, and nutritional value. The integration of transcriptomics and metabolomics has emerged as a transformative strategy, enabling the identification of hub genes and metabolites that coordinately regulate key quality traits. For instance, in grass carp, combined analysis revealed that PPARγ-mediated lipid metabolism governs both collagen deposition and n-3 Polyunsaturated fatty acids (n-3 PUFAs) retention, directly impacting muscle firmness and oxidative stability (Yu et al., 2024). Based on a combined transcription-metabolism analysis, the HIF-1α pathway-mediated hypoxic stress was found to be a central mechanism for the decline in muscle quality of tilapia under high-density culture conditions (Li et al., 2018). Despite these methodological advances, the application of integrated multi-omics approaches is still limited in deciphering the transcriptional regulation and metabolic interactions that underlie muscle quality differences between wild-type and aquaculture-improved fish variants. Current studies mainly emphasize environmental regulators (e.g. stocking density) and nutritional interventions, while the regulatory mechanisms between genetic mutations (especially those associated with pigmentation) and biochemical remodeling are severely understudied. Recently, Integrated transcriptomic and metabolomic profiling revealed the effects of astaxanthin on the growth and body color of Leopard Coral Grouper (*Plectropomus leopardus*) (Zhu et al., 2021), highlighting the untapped potential of integrated multi-omics analyses in resolving phenotypic differences in aquaculture breeding.

In this study, we employed an integrated multi-omics strategy combining untargeted LC-MS metabolomics and RNA-seq to systematically characterize metabolic and transcriptional disparities in muscle tissues between YM and WT snakeheads. Metabolomics analysis identified metabolic profiles, differential metabolites (DMs), and associated metabolic pathways. RNA-seq analysis provided insights into gene expression profiles, differentially expressed genes (DEGs), and relevant regulatory pathways. Additionally, the integrative analysis of transcriptomic and metabolomic data was conducted to explore the relationship between metabolites and genes, revealing key regulatory pathways responsible for the differences between the muscle tissues of YM and WT snakeheads. The results contribute to understanding the variations in flesh quality between the two strains and evaluating the economic potential of the YM snakehead in aquaculture, providing a theoretical basis for the farming and breeding industries.

2. Materials and methods

2.1. Sample collection

Juvenile WT and YM snakeheads (4 months old, 105 ± 12 g) used in this experiment were collected from Linyi, Shandong Province, China. Three identical ponds each for YM and WT snakeheads were used as experimental replicate groups. Throughout the 4-month aquaculture cycle, the YM and WT strains of snakeheads were reared under identical culture conditions and feed composition. The stocking density was maintained at 15,000 individuals per hectare (ind./ha), with pelleted feed containing 45 % crude protein administered twice daily at a ration equivalent to 2.5 % of total fish body weight. Three fish were randomly caught from each group, for a total of 18 experimental fish, and all experimental fish were anesthetized using tricaine methanesulfonate (MS-222, 150 mg/L) and subsequently euthanized. Bilateral skeletal muscle tissues were aseptically excised from the epaxial musculature and partitioned into two aliquots: one aliquot was immediately flash-frozen in liquid nitrogen and archived at −80 °C for subsequent multi-omics profiling (metabolomics and transcriptomics), while the parallel aliquot was preserved at −20 °C for comprehensive flesh quality assessment, including texture profile analysis and biochemical characterization. All animal handling and sample collection procedures were approved by the Animal Research and Ethics Committee of Ocean University of China.

2.2. Flesh quality measurement of WT and YM snakeheads

Flesh quality indexes of WT and YM snakehead muscle samples (n = 9 for each type) were measured, including proximate composition, muscle color, fatty acid composition, and volatile compounds (VOCs) composition. Proximate composition analysis was conducted using the AOAC methods to determine moisture, crude ash, crude protein, and crude fat (AOAC, 1990). Moisture content was measured by drying samples in an oven at 105 °C until a constant weight was achieved. Crude ash content was determined using a muffle furnace at 550 °C. Crude protein and crude fat contents were measured using the Kjeldahl method and the Soxhlet method, respectively.

Muscle color was evaluated using the Lab* color system, where L* indicates brightness, a* indicates redness, and b* indicates yellowness. The parameters of each fresh muscle sample were measured using a CS-10 colorimeter (CHN Spec, Hangzhou, China), with the mean calculated from three repeated measurements.

For fatty acid composition analysis, freeze-dried muscle samples were converted into fatty acid methyl esters (FAMEs) using the HCl-methanol method. FAMEs were quantified using an HP6890 gas chromatograph (Agilent Technologies, Santa Clara, USA) equipped with a flame ionization detector and a fused silica capillary column (007-CW, Hewlett Packard, Palo Alto, USA). Experimental procedures followed the methods outlined by Zuo et al. (2012).

In the VOCs composition analysis, 2.00 g of freeze-dried muscle samples were accurately weighed and placed in a 15 mL headspace vial. VOCs were extracted via solid-phase microextraction (SPME) using a 65 μm DVB-PDMS fiber (Supelco, Bellefonte, USA). The SPME fiber was exposed to the sample headspace at 60 °C for 30 min, then transferred to the injector for desorption at 250 °C for 5 min. GC-MS analysis was performed using a GCMS-QP2010 plus (Shimadzu, Kyoto, Japan) with a

CD-5 MS capillary column (30 m × 0.25 mm, 0.25 μm). The detection conditions were as follows: carrier gas: helium; flow rate: 1.0 mL/min (splitless mode); temperature program: initial 35 °C for 1 min, ramping to 60 °C at 5 °C/min, holding for 1 min, increasing to 140 °C at 6 °C/min, holding for 1 min, then heating to 230 °C at 8 °C/min, holding for 5 min; ion source temperature: 200 °C; electron energy: 70 eV; mass scan range: 35–350 m/z. VOCs were identified using the National Institute of Standards and Technology (NIST 17) database, and the relative contents of VOCs were calculated using the peak area normalization method.

To identify key odor compounds, the relative odor activity value (ROAV) was calculated to assess the contribution of each VOC to the overall flavor. The formula for ROAV is as follows:

$$ROAV_i \approx \frac{C_i}{C_{max}} \times \frac{T_{max}}{T_i} \times 100$$

$ROAV_i$ represents the ROAV of arbitrary VOC; C_i and T_i denote the relative concentration and sensory threshold of arbitrary VOC, respectively; C_{max} and T_{max} refer to the relative concentration and sensory threshold of the highest contributing VOC to the overall flavor, respectively.

2.3. Metabolite extraction and untargeted LC-MS analysis

All samples (WT n = 7, YM n = 8) were accurately weighed to 30 mg and transferred to 1.5-mL Eppendorf tube. Each tube received two small steel balls, 20 μL of an internal standard (2-chloro-L-phenylalanine in methanol, 0.3 mg/mL), and 400 μL of an extraction solvent composed of methanol and water (4:1, v/v). Samples were stored at −20 °C for 2 min, ground at 60 Hz for 2 min, ultrasonicated for 10 min, and then stored at −20 °C for an additional 30 min. The extract was centrifuged at 13,000 rpm and 4 °C for 15 min, and 300 μL of the supernatant was dried in LC-MS vials. To each sample, 200 μL of a methanol-water mixture (1:4, v/v) was added, followed by vortexing for 30 s and ultrasonication for 3 min. Samples were then placed at −20 °C for 2 h, centrifuged at 13,000 rpm and 4 °C for 5 min, and the supernatants (150 μL) were collected using crystal syringes. These were filtered through 0.22 μm microfilters and transferred to LC vials, which were stored at −80 °C until LC-MS analysis. Three quality control (QC) samples were prepared by mixing aliquots of all samples to create a pooled sample. The QCs were injected at regular intervals (every 6 samples) throughout the analytical run to assess repeatability. Water, methanol, acetonitrile, and formic acid were purchased from CNW Technologies GmbH (Düsseldorf, Germany), while 2-chloro-L-phenylalanine was sourced from Shanghai Hengchuang Biotechnology Co., Ltd. (Shanghai, China). All chemicals were of analytical or HPLC grade.

An AB SCIEX ExionLC system coupled with an AB SCIEX Triple TOF 6600 Plus System (AB SCIEX, Framingham, USA) was employed to analyze metabolic profiling in both positive ion mode (ESI+) and negative ion mode (ESI-), utilizing an ACQUITY UPLC HSS T3 column (100 mm × 2.1 mm, 1.8 μm). The binary gradient elution system consisted of solvent A (0.1 % formic acid in water, v/v) and solvent B (0.1 % formic acid in acetonitrile, v/v), with separation achieved using the following gradient: 0 min, 5 % B; 2 min, 5 % B; 4 min, 30 % B; 8 min, 50 % B; 10 min, 80 % B; 14 min, 100 % B; 15 min, 100 % B; 15.1 min, 5 % B; and 16 min, 5 % B. The flow rate was set at 0.35 mL/min, and the column temperature was maintained at 45 °C. The injection volume was 2 μL.

Data acquisition was performed using TOF MS scan mode (m/z range: 100 to 1000). The parameters for mass spectrometry were as follows: nebulizer gas (GS1), 55 PSI (+) and 55 PSI (−); auxiliary gas (GS2), 55 PSI (+) and 55 PSI (−); curtain gas (CUR), 35 PSI (+) and 35 PSI (−); ion source temperature, 550 °C (+) and 550 °C (−); ion spray voltage, 5500 V (+) and −4500 V (−); declustering potential, 80 V (+) and −80 V (−); collision energy, 10 eV (+) and −10 eV (−); and interface heater temperature, 550 °C (+) and 550 °C (−). For product ion scan mode, the m/z range was set from 40 to 1000, with a collision energy of 35 eV (+) and −35 eV (−).

The acquired untargeted LC-MS metabolomic raw data were analyzed using Progenesis QI 2.3 software (Nonlinear Dynamics, Newcastle, UK), and metabolites were identified utilizing the Human Metabolome Database (HMDB), Lipid MAPS Structure Database (LMSD), and METLIN database (http://www.hmdb.ca/, http://www.lipidmaps.org/, https://metlin.scripps.edu/).

2.4. Data processing of metabolomic analysis

The data matrix was imported into the ropls R package (v 1.28.2) for principal component analysis (PCA) and orthogonal partial least-squares-discriminant analysis (OPLS-DA). In OPLS-DA, a 7-fold cross-validation and 200 iterations of response permutation testing (RPT) were employed to prevent overfitting and evaluate model quality. Additionally, univariate statistical analysis was conducted, including student's t-test and fold change analysis.

Metabolites with a variable importance of projection (VIP) greater than 1 in the OPLS-DA and a *P*-value less than 0.05 in the student's t-test were classified as DMs. The Kyoto Encyclopedia of Genes and Genomes (KEGG) database (http://www.genome.jp/kegg/) was utilized for metabolite annotation of the DMs, and OECloud tools (https://cloud.oebiotech.cn) were used for KEGG pathway enrichment analysis.

2.5. RNA extraction and RNA-seq analysis

Total RNA from muscle samples (nine samples per group) was extracted using TRIzol reagent (Vazyme Biotech, Nanjing, China). The concentration and integrity of the total RNA were assessed using a NanoDrop 2000 (Thermo Scientific, Waltham, USA) and agarose gel electrophoresis. Nine RNA samples from the same experimental group were divided into three subsets, and each subset containing three samples was pooled in equal RNA quantities to generate three biological replicates. A total of six RNA samples (WT n = 3, YM n = 3) were used to generate sequencing libraries and sequenced on the Illumina NovaSeq 6000 platform with 150 bp paired-end reads. The transcriptome data were submitted to the National Center for Biotechnology Information (NCBI), with the Sequence Read Archive (SRA) accession number PRJNA877371. Quality control and filtering of the raw data were performed using Fastp (v 0.12.4) to obtain clean reads. Subsequently, the clean reads were aligned to the *C. argus* reference genome (GenBank accession GCA_027943205.2) using Hisat2 (v 2.2.1). StringTie (v 2.1.5) was employed to calculate normalized gene expression levels as fragments per kilobase of transcript per million mapped reads (FPKM). The DESeq2 R package (v 1.36.0) was used for differential expression analysis. Genes with an adjusted *P*-value (*P*-adj) less than 0.05 and |log2(fold change)| greater than 1 were considered as DEGs. Additionally, KOBAS (http://kobas.cbi.pku.edu.cn/) was utilized for KEGG pathway enrichment analysis.

Quantitative real-time PCR (qPCR) analysis of the pooled RNA samples was performed to verify the accuracy of RNA-seq results. cDNA was synthesized using HiScript® III RT SuperMix for qPCR (+gDNA wiper) (Vazyme Biotech, Nanjing, China). The expression levels of selected genes (*pnpla7*, *gpat3*, *hspb11*, *mat2a*, *adss2*, *sod1*, *prdx5*, *ndufb3*, *gpx1*, *β-actin*) were quantified by qPCR. Primers were designed using Primer 5.0 software and are listed in Table S1. The qPCR reaction used ChamQ™ SYBR® Color qPCR Master Mix (High ROX Premixed) (Vazyme Biotech, Nanjing, China) and contained 1 μL cDNA, 0.2 μL forward primer, 0.2 μL reverse primer, 5 μL 2 × ChamQ SYBR Color qPCR Master Mix, and 3.6 μL nuclease-free water. qPCR amplification was performed on the StepOne Plus Real-Time PCR system (Applied Biosystems, Foster City, CA, USA) with the following conditions: 95 °C for 30 s, followed by 40 cycles at 95 °C for 10 s, Tm for 30 s, and 72 °C for 30 s. *β-actin* was used as the internal control, and the WT group served as the control group. Relative expression levels were calculated using the $2^{-\Delta\Delta Ct}$ method.

2.6. Combined transcriptomic and metabolomic analysis

Pearson correlation coefficients (*r*) between DEGs and DMs were calculated by the stats R package (v 4.0.3). All significant metabolites (VIP >1) and DEGs were used for joint-pathway enrichment analysis via MetaboAnalyst (https://www.metaboanalyst.ca/). Key regulatory pathways were identified, and schematic diagrams were generated to illustrate these pathways. Additionally, the correlation between significant genes (*P*-adj <0.05) and metabolites (VIP >1) associated with these pathways was visualized.

2.7. Myoglobin derivatives relative content measure

The myoglobin derivatives assessed in this study included deoxymyoglobin (deoMB), oxymyoglobin (oxyMB), and metmyoglobin (metMB). For the measurement of their relative contents, 2.00 g of fresh muscle samples were accurately weighed and placed in a 50 mL centrifuge tube containing 20 mL of phosphate buffer (pH 6.8, 40 mM, 4 °C). The samples were homogenized and centrifuged at 10,000 r/min for 30 min at 4 °C. The supernatant was then filtered through a 0.22 μm membrane, and the absorbance at 572 nm, 565 nm, 545 nm, and 525 nm was measured using a spectrophotometer, with 40 mM phosphate buffer as the blank control. The relative content of myoglobin derivatives was calculated using the formula provided by Krzywicki (1982) as follows:

$$metMB\% = (-2.514*R_1+0.777*R_2+0.8*R_3+1.098)*100$$

$$deoMB\% = (0.369*\ R_1+1.140*R_2-0.941*R_3+0.015)*100$$

$$oxyMB\% = (0.882*R_1-1.267*R_2+0.809*R_3-0.361)*100$$

$$R1 = A_{572}/A_{525},\ R2 = A_{565}/A_{525},\ R3 = A_{545}/A_{525}$$

2.8. Statistical analysis

All experiments were performed at least in triplicate to ensure statistical robustness. Following confirmation of normality (Shapiro-Wilk test), the differences among the mean values were analyzed using Duncan's multiple-range test. Treatment means were tested separately for least significant difference (LSD) using SPSS 25.0 statistical software (IBM, USA). The significance level was set at $P < 0.05$.

3. Results

3.1. Phenotypic characterization of muscle quality in YM and WT snakeheads

The proximate composition showed no significant differences between YM and WT snakeheads (Fig. 1C, Table S2). However, muscle color analysis revealed that the a* value (redness) was significantly

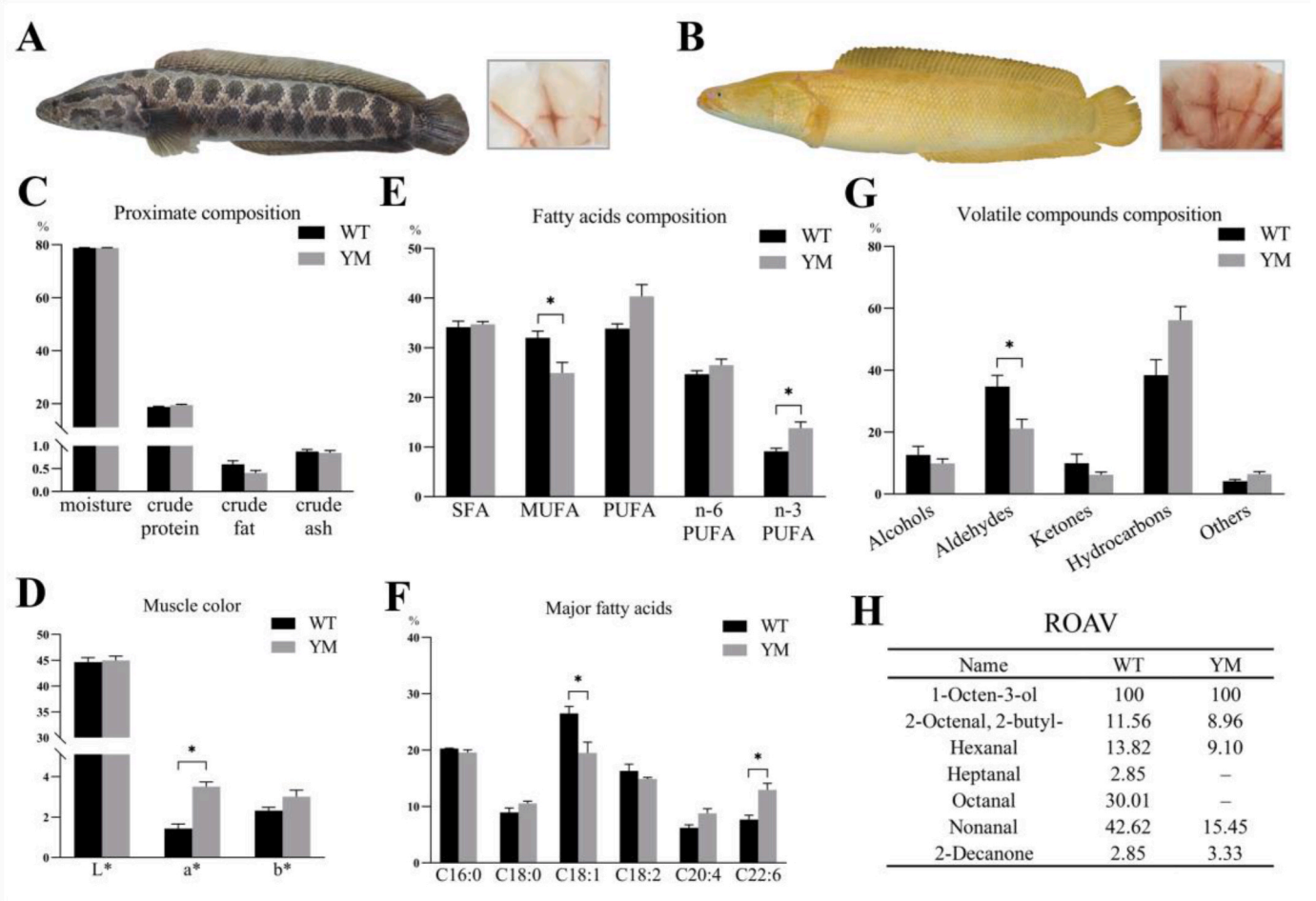

Name	WT	YM
1-Octen-3-ol	100	100
2-Octenal, 2-butyl-	11.56	8.96
Hexanal	13.82	9.10
Heptanal	2.85	–
Octanal	30.01	–
Nonanal	42.62	15.45
2-Decanone	2.85	3.33

Fig. 1. Comparative analysis of flesh quality in YM vs WT snake**heads. (A)** The body and muscle color of YM snakehead. **(B)** The body and muscle color of WT snakehead. **(C)** Proximate composition indexes between YM and WT snakeheads. **(D)** Muscle color parameters between YM and WT snakeheads. **(E)** Fatty acids composition between YM and WT snakeheads. **(F)** The content of major fatty acids between YM and WT snakeheads. **(G)** VOCs composition between YM and WT snakeheads. **(H)** ROAV of key odor compounds.
Notes: *, the difference between two groups is significant at the 0.05 level.

higher in YM snakehead ($P < 0.05$) (Fig. 1D–Table S2), a trait directly linked to consumer preference for freshness.

Fatty acid composition analysis indicated that PUFAs dominated in YM muscle (40.34 % of total fatty acids), whereas saturated fatty acids (SFAs) were predominant in WT (34.14 %) (Fig. 1E–Table S2). Notably, YM snakehead displayed a 1.51-fold higher n-3 PUFA content ($P < 0.05$), particularly docosahexaenoic acid (DHA, C22:6, 1.68-fold), alongside reduced monounsaturated fatty acids (MUFAs) compared to WT snakehead ($P < 0.05$) (Fig. 1E and F, Table S2).

In terms of VOCs, 46 VOCs were detected in YM snakehead, and 48 in WT snakehead. The VOCs included 6 alcohols, 11 aldehydes, 4 ketones, 24 hydrocarbons, and 6 other compounds (Table S3). WT snakehead muscle contained significantly higher aldehyde levels ($P < 0.05$), contributing to its pronounced fishy odor (Fig. 1G–Table S3). In contrast, YM muscle was enriched in hydrocarbons, which are associated with milder flavor profiles. ROAV analysis identified 1-octen-3-ol as the dominant odorant (ROAV = 100), with additional key contributors including 2-butyl-2-octenal and 2-decanone (Fig. 1H–Table S4). These findings suggest that lipid oxidation products (e.g., aldehydes) drive flavor divergence between the two strains.

3.2. Metabolite identification in muscle of YM and WT snakeheads

Untargeted LC-MS metabolomics analysis was performed on muscle samples from both YM and WT snakeheads. A series of peak intensities were visualized on total ion chromatograms (TIC) for both YM and WT groups in ESI+ and ESI- modes (Fig. S1). The peaks from all samples were subjected to PCA, which revealed that the QC samples clustered closely, indicating good instrument stability and reliable analysis (Fig. 2A). Multivariate analysis (PCA, OPLS-DA) confirmed robust separation between YM and WT groups, validating metabolic distinctness (Fig. S2). The PCA score plot showed clear separation between the two groups along PC1, indicating significant differences in muscle tissue between YM and WT snakeheads (Fig. S2A). Similarly, the OPLS-DA score plot demonstrated a clear distinction between the two groups, indicating significant differences in their metabolomic profiles (Figs. S2B–C).

Untargeted LC-MS metabolomics identified 1021 metabolites, with lipids and lipid-like molecules constituting the largest class (43.88 %, Fig. 2B). The results of multivariate and univariate statistical analyses were visualized using a volcano plot (Fig. 2C). Metabolites with *P*-value <0.05 and VIP >1 were considered significantly different, with $\log_2$(fold change) > 0 indicating upregulation and $\log_2$(fold change) < 0 indicating downregulation in YM snakehead. A total of 137 metabolite peaks showed significant differences between YM and WT snakeheads, and 42 DMs were identified through database annotation (Table 1).

3.3. Differential metabolites analysis of muscle between YM and WT snakeheads

Hierarchical clustering heatmaps were used to illustrate the expression of DMs in each sample (Fig. 2D). A total of 10 metabolites, including

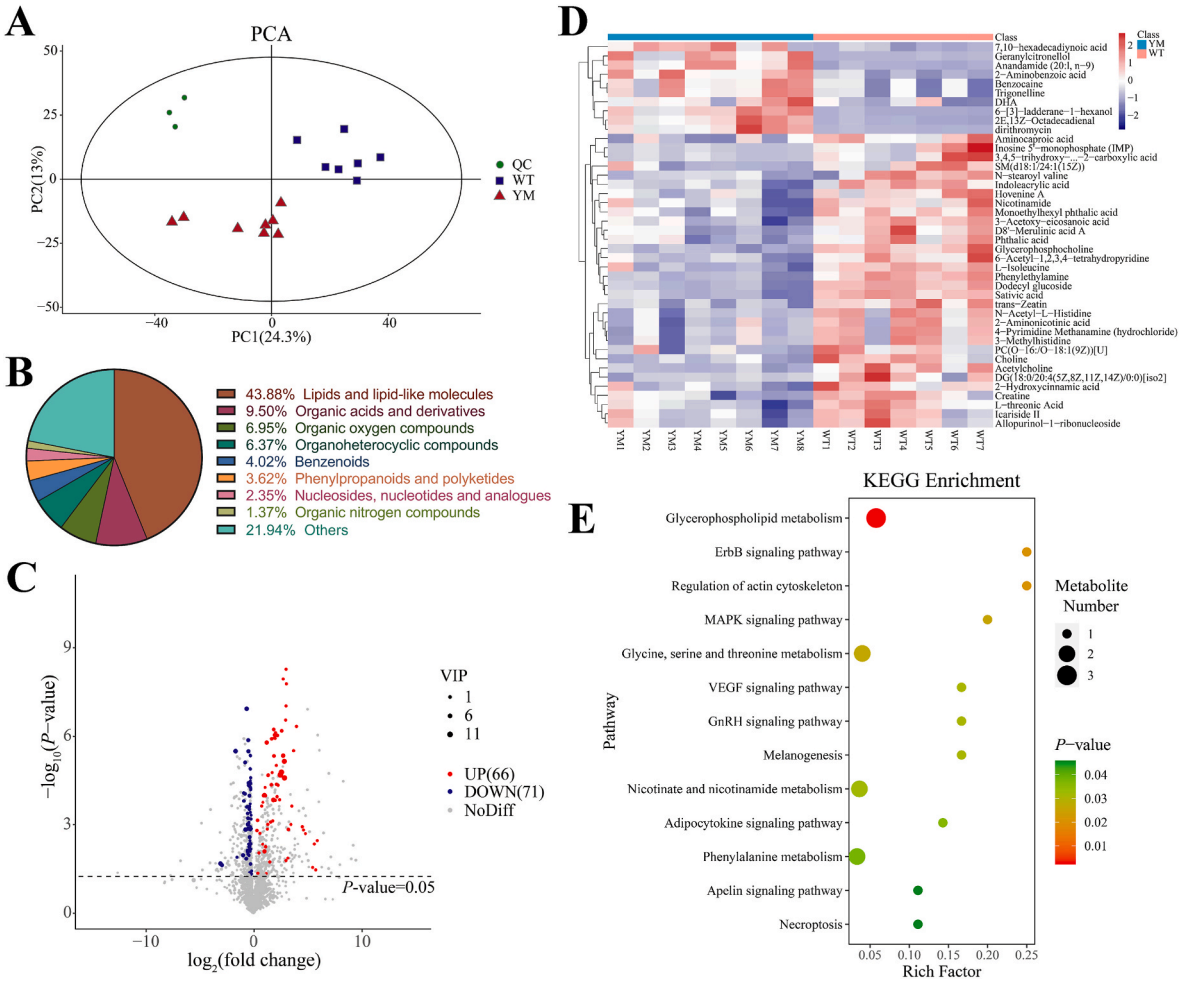

Fig. 2. Differential metabolites analysis of muscle between YM and WT snake**heads. (A)** The PCA score plot of metabolomic in QC, YM, and WT groups. **(B)** The composition of the metabolites based on the databases. **(C)** The volcano plot of the metabolite peaks. **(D)** The hierarchical clustering heatmap of the DMs. **(E)** KEGG pathway enrichment of the DMs.

Table 1
The identification of DMs in muscle of YM and WT snakeheads.

Metabolites	Retention time (min)	Mass charge ratio (m/z)	VIP	*P*-value	log_2(fold change)
ESI+					
Glycerophosphocholine	0.77	258.11	9.2521	0.0000	−1.6177
N-Acetyl-L-Histidine	0.93	198.09	8.6587	0.0014	−0.6934
2E,13Z-Octadecadienal	13.21	282.28	7.6180	0.0001	1.8771
Dodecyl glucoside	15.16	387.21	7.2962	0.0000	−0.6008
Creatine	0.87	132.08	7.1462	0.0074	−0.3413
Benzocaine	6.12	166.09	6.6622	0.0080	1.0521
Phenylethylamine	14.20	122.10	5.9570	0.0000	−0.4373
3,4,5-trihydroxy-6-(1-oxo-1H-isochromene-3-carbonyloxy)oxane-2-carboxylic acid	1.21	349.06	5.4967	0.0235	−2.8817
Icariside II	2.25	537.17	5.1539	0.0468	−0.2121
D8′-Merulinic acid A	15.50	391.29	4.7548	0.0027	−0.3302
SM(d18:1/24:1(15Z))	13.30	813.68	4.4072	0.0142	−0.6483
Sativic acid	13.92	387.21	4.3570	0.0000	−0.4660
L-threonic Acid	2.25	137.05	4.2394	0.0044	−0.2556
Geranylcitronellol	14.37	310.31	3.1063	0.0014	3.2439
Allopurinol-1-ribonucleoside	2.25	269.09	3.0651	0.0216	−0.2494
Acetylcholine	0.90	146.12	2.5846	0.0002	−0.8732
N-stearoyl valine	14.02	384.35	2.2303	0.0080	−0.3081
Indoleacrylic acid	4.24	188.07	2.1986	0.0004	−0.5337
Nicotinamide	1.31	123.06	2.1848	0.0109	−0.4043
6-[3]-ladderane-1-hexanol	12.43	280.26	2.1539	0.0001	2.1914
trans-Zeatin	3.81	220.12	2.0905	0.0001	−0.8843
Trigonelline	6.12	138.05	2.0071	0.0057	1.1408
Hovenine A	0.86	525.29	1.8640	0.0053	−0.3215
DG(18:0/20:4(5Z,8Z,11Z,14Z)/0:0)[iso2]	13.29	627.54	1.7896	0.0128	−1.5139
PC(O-16:/O-18:1(9Z))[U]	13.92	770.58	1.7203	0.0423	−0.3498
2-Aminonicotinic acid	0.93	156.08	1.6653	0.0077	−0.5639
4-Pyrimidine Methanamine (hydrochloride)	0.93	110.07	1.6568	0.0075	−0.5535
Choline	0.77	104.11	1.5787	0.0013	−0.4905
L-Isoleucine	2.20	132.10	1.4769	0.0002	−0.5582
2-Hydroxycinnamic acid	2.05	182.08	1.3864	0.0098	−0.5048
2-Aminobenzoic acid	2.37	138.05	1.3181	0.0008	1.7857
Dirithromycin	13.21	563.55	1.2573	0.0010	3.4761
Anandamide (20:l, n-9)	13.48	354.34	1.2538	0.0001	2.4347
Phthalic acid	15.50	149.02	1.2426	0.0069	−0.2418
3-Methylhistidine	0.93	152.08	1.2126	0.0084	−0.5632
3-Acetoxy-eicosanoic acid	15.54	371.32	1.1196	0.0004	−0.2824
Aminocaproic acid	4.45	114.09	1.0872	0.0099	−0.5176
6-Acetyl-1,2,3,4-tetrahydropyridine	13.87	108.08	1.0483	0.0012	−0.2570
Monoethylhexyl phthalic acid	11.73	279.16	1.0183	0.0015	−0.4073
ESI-					
Inosine 5′-monophosphate (IMP)	1.24	347.04	6.5732	0.0208	−3.0323
DHA	12.96	327.23	1.7696	0.0446	0.4249
7,10-hexadecadiynoic acid	9.72	293.17	1.4753	0.0008	1.5944

2E,13Z-octadecadienal, benzocaine, geranylcitronellol, 6-[3]-ladderane-1-hexanol, trigonelline, DHA, 7,10-hexadecadiynoic acid, 2-aminobenzoic acid, dirithromycin, and anandamide (20:1, n-9), formed one cluster with higher expression in the YM snakehead. The remaining 32 metabolites comprised another cluster with higher expression in the WT snakehead (Fig. 2D). KEGG pathway enrichment analysis was conducted to explore potential metabolic differences in muscle tissue between YM and WT snakeheads. The results indicated that DMs were annotated into 13 significantly enriched metabolic pathways (*P*-value <0.05) (Fig. 2E). The most significant pathway was "Glycerophospholipid metabolism," which included three metabolites, while "Glycine, serine and threonine metabolism," "Nicotinate and nicotinamide metabolism," and "Phenylalanine metabolism" each contained two metabolites.

3.4. Differentially expressed genes identification in muscle of YM and WT snakeheads

RNA-seq analysis was performed on muscle samples from YM and WT snakeheads, yielding a total of 123.94 million clean reads after filtering. The Q20 and Q30 values reached 99.49 % and 96.35 %, respectively, with the GC percentage ranging from 49.71 % to 50.25 %. The total mapped rate to the reference genome exceeded 95.79 % (Table S5), indicating the reliability of the RNA-seq data for subsequent analyses.

Following expression analysis, 15,790 genes were co-expressed in both YM and WT snakeheads, while 1021 and 875 genes were uniquely expressed in YM and WT snakeheads, respectively. A total of 380 DEGs were identified (*P*-adj <0.05, |log2(fold change)| > 1), comprising 163 up-regulated genes and 217 down-regulated genes in the YM snakehead (Table S6). The volcano plot (Fig. 3A) and hierarchical clustering heatmap (Fig. S3A) were utilized to visualize the expression levels of the DEGs. To validate the RNA-seq results, 9 genes were randomly selected for qPCR analysis, with relative expression levels consistent with RNA-seq findings ($R^2 = 0.9022$) (Fig. S3B).

To investigate the molecular mechanisms underlying muscle tissue differences between YM and WT snakeheads, all DEGs underwent KEGG enrichment analysis. The results revealed significant enrichment in 16 KEGG pathways (*P*-value <0.05), with the "Ribosome" pathway being the most prominent. Other significant pathways included "Adrenergic signaling in cardiomyocytes", "Oxidative phosphorylation", "MAPK signaling pathway", "Phagosome", "Cell adhesion molecules", "Focal adhesion", as well as metabolic pathways such as "Riboflavin metabolism", "Glutathione metabolism", and "Nitrogen metabolism" (Fig. 3B).

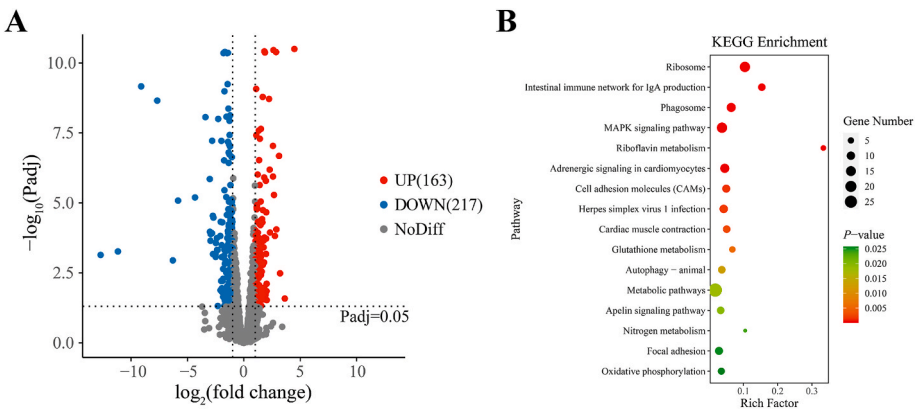

Fig. 3. Differentially expressed genes identification in muscle of YM and WT snake**heads. (A)** The volcano plot of the genes. **(B)** KEGG pathway enrichment of the DEGs.

3.5. Integrative analysis of transcriptomic and metabolomic in muscle of YM and WT snakeheads

To explore the joint effects of genes and metabolites on flesh quality between YM and WT snakeheads, a total of 380 DEGs and 42 DMs were subjected to correlation analysis. The heatmap displayed clusters of up-regulated DEGs and DMs, as well as a separate cluster for down-regulated DEGs and DMs (Fig. S4). Strong correlations ($|r| > 0.8$) between DEGs and DMs are listed in Table S7. Furthermore, joint-pathway enrichment analysis was conducted to comprehensively investigate the molecular mechanisms regulating flesh quality differences. Metabolites with VIP >1, deemed important contributors to the differences in the OPLS-DA model, were subjected to joint-pathway enrichment analysis alongside the DEGs. The enriched pathways are shown in Fig. 4A, including "Cardiac muscle contraction", "MAPK signaling pathway", and "Glycerophospholipid metabolism", etc, with details listed in Table S8.

3.6. Mechanism of lipid metabolism and muscle color differences

Our analysis identified "Glycerophospholipid metabolism" and "Regulation of lipolysis in adipocytes" as key regulatory pathways associated with lipid metabolism differences. These pathways are illustrated in the schematic diagram (Fig. 4B). The correlation between important genes (*pnpla6*, *pnpla7*, *gapat3*, *prkg2*, *lipe*) and metabolites (acetylcholine, choline, glycerophosphocholine, PC(14:0/20:1(11Z)), PS(O-16:0/18:0), PS(O-16:0/22:1(11Z)), PC(22:6(4E,7E,10E,13E,16E,19E)/0:0), LysoPC(22:6(4Z,7Z,10Z,13Z,16Z,19Z)), LysoPC(18:2(9Z,12Z)), PC(18:1(6Z)/0:0), DG(18:0/20:4(5Z,8Z,11Z,14Z)/0:0)[iso2], PE(0:0/22:6(4Z,7Z,10Z,13Z,16Z,19Z)), PC(20:5(5Z,8Z,11Z,14Z,17Z)/22:2(13Z,16Z)), PC(O-16:/O-18:1(9Z))[U], PI(O-20:0/16:0), PE(16:0/0:0)) related to lipid metabolism is shown in Fig. 4C.

Moreover, "Nicotinate and nicotinamide metabolism" was identified as a key pathway regulating muscle color. This pathway influences the synthesis and content of NAD^+ and $NADP^+$, which subsequently affects the expression of genes involved in oxidative phosphorylation, peroxisome function, and glutathione metabolism, ultimately resulting in changes in muscle color. The details of this process are illustrated in the schematic diagram (Fig. 5A), with correlations among key genes (*atp5f1e*, *atp5po*, *ndufb3*, *uqcrq*, *mt-nd5*, *sod1*, *prdx5*, *gpx1*, *gpx8*, *gstt2b*, *rrm1*, *ggt7*) and metabolites (nicotinamide, trigonelline, glutathione) presented in Fig. 5B. In addition, the metMB content in the muscle of YM snakehead was significantly higher than that of the WT ($P < 0.05$) (Fig. 5C), and the schematic diagram depicting changes in the relative content of myoglobin derivatives is shown in Fig. 5D.

4. Discussion

4.1. Differences in flesh quality

Fish flesh quality is a significant concern in aquaculture, attracting considerable interest from researchers and consumers (Lv et al., 2021). In this study, we measured the chemical composition, color, and flavor of snakehead muscle tissue to evaluate the differences in flesh quality between YM and WT snakeheads. The proximate composition of YM and WT snakeheads was similar, likely due to comparable environmental and dietary conditions. However, YM snakehead exhibited significantly redder muscle compared to WT, which may be favored by consumers, as muscle color serves as a direct sensory indicator of flesh quality. Fatty acid composition significantly impacts nutritional value. The higher content of n-3 PUFAs, particularly DHA, in YM snakehead indicates enhanced nutritional benefits, such as improved brain function and reduced risks of thrombosis and hypertension (Horrocks & Yeo, 1999).

Flavor profiles are largely determined by VOCs. ROAV analysis revealed that WT snakehead had higher quantities and ROAV values of key odor compounds, including aldehydes, ketones, and alcohols, which are the primary contributors to the fishy odor (Liu et al., 2021). The milder hydrocarbons in YM snakehead suggest a more acceptable flavor profile for consumers. PUFA oxidation is a major source of these undesirable odors, indicating a direct correlation between fatty acid and VOC compositions in both snakehead varieties. Notably, YM snakehead had higher levels of pyrazines, which contribute desirable roasted flavors (Yu et al., 2021).

4.2. Metabolite differences and their biological significance

To further understand the biochemical basis of flesh quality differences, we conducted a metabolomic analysis of YM and WT snakehead muscles. This analysis provides insights into the specific metabolic alterations associated with phenotype differences. Our metabolomic analysis identified 1021 metabolites, including 42 DMs between YM and WT snakeheads. "Lipids and lipid-like molecules" were the most abundant class, playing a crucial role in the metabolic profiles of snakehead muscle tissue. Fatty acyls, primarily responsible for ATP synthesis via β-oxidation (Calvani et al., 2000), were prevalent among the DMs. Other significant DMs included benzenoids, organoheterocyclic compounds, and organic acids. PC, DHA, DG, anandamide, acetylcholine, and some other DMs were also identified in LC-MS metabolomics analysis of grass carp muscle (Zhao, Chong, et al., 2018). So these DMs could be used as potential biomarkers to distinguish two snakeheads.

Noteworthy DMs included DHA, anandamide (20:1, n-9), and trigonelline, which were up-regulated in YM snakehead. The abundance of DHA corroborates the fatty acid composition findings. Anandamide, an

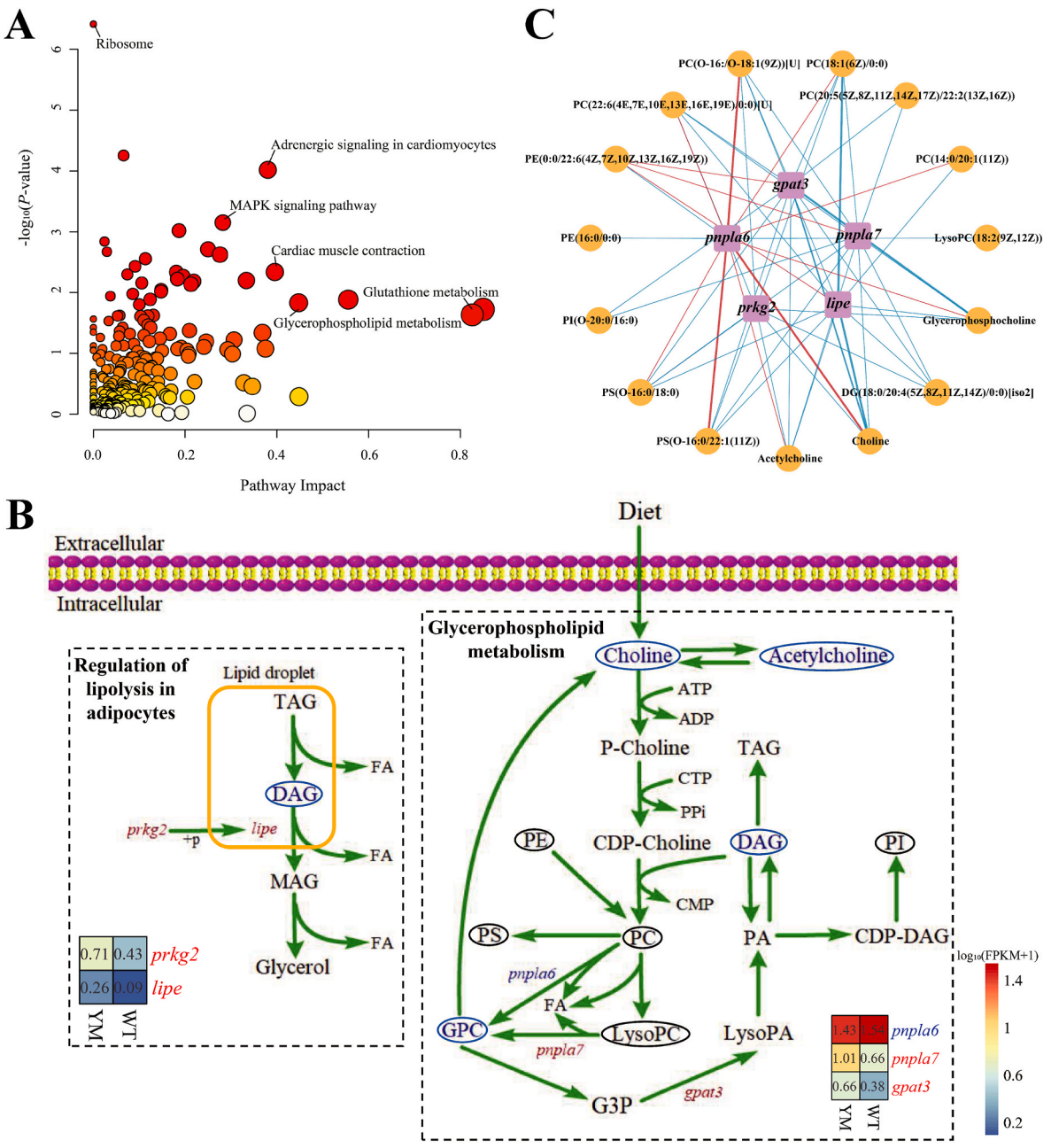

Fig. 4. Schematic diagram reveals predicted molecular mechanism of lipid metabolism differences. **(A)** Joint-pathway enrichment of the DEGs and the important metabolites. **(B)** Schematic diagram of related pathways. The heatmap indicates the expression levels of the related genes. **(C)** The correlation network graph of the important genes and metabolites related to lipid metabolism.

Notes: P-choline, phosphocholine; PC, phosphatidylcholine; LysoPC, lysophosphatidylcholine; GPC, glycerophosphocholine; G3P, glycerol 3-phosphate; PA, phosphatidic acid; LysoPA, lysophosphatidic acid; PI, phosphatidylinositol; PE, phosphatidylethanolamine; PS, phosphatidylserine; TAG, triacylglycerol; DAG, diacylglycerol; MAG, monoacylglycerol.

endocannabinoid, binds to cannabinoid receptors, influencing signal transmission (Astarita et al., 2008). Trigonelline is known for its neuroprotective and anticancer properties (Ashihara et al., 2015). In contrast, inosine 5′-monophosphate (IMP) and creatine showed significantly higher expression in WT snakehead. IMP, an umami substance, is widely used as a flavor enhancer (Kuchiba-Manabe et al., 1991) and enhances umami taste in combination with sweet and acidic amino acids (Kawai et al., 2002). Creatine, synthesized from glycine and methionine (Meléndez-Hevia et al., 2009), plays a crucial role in muscle energy metabolism.

Some metabolites, such as nicotinamide and glycerophosphocholine, are vital for regulating muscle quality, with further exploration required through integrative analysis of transcriptomic and metabolomic data. Despite identifying 1021 metabolites, limitations exist; some metabolites remained unclassified, and high molecular weight and volatile metabolites may have been overlooked (Xiao et al., 2020).

4.3. *Differentially expressed genes and their functions*

To complement the metabolomics data and explore the genetic mechanisms underlying the observed phenotypic differences, transcriptomic analysis was performed. This approach allowed us to identify DEGs related to muscle structure and metabolism. The transcriptomic analysis revealed 380 DEGs between YM and WT snakeheads. Notably,

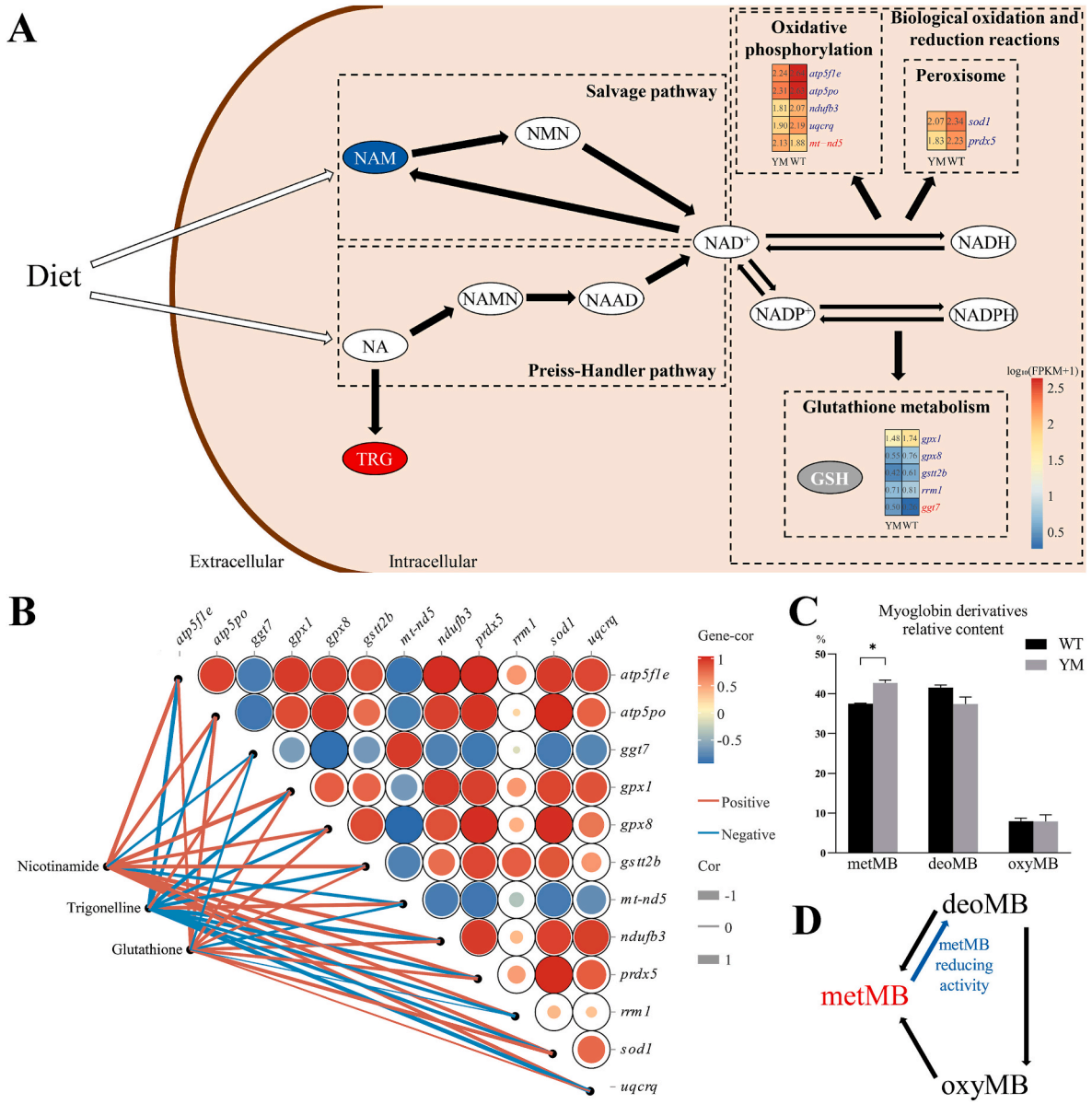

Fig. 5. Schematic diagram reveals predicted molecular mechanism of muscle color differences. **(A)** Schematic diagram of related pathways. The heatmap indicates the expression levels of the related genes. **(B)** Correlation of the important genes and metabolites related to muscle color. **(C)** The myoglobin derivatives relative content between YM and WT snakeheads. **(D)** Schematic diagram of changes in the relative content of myoglobin derivatives.
Notes: *, the difference between two groups is significant at the 0.05 level.NA, nicotinic acid; TRG, trigonelline; NAMN, nicotinic acid mononucleotide; NAAD, nicotinic acid adenine dinucleotide; NAM, nicotinamide; NMN, nicotinamide mononucleotide; NAD^+, nicotinamide adenine dinucleotide; $NADP^+$, nicotinamide adenine dinucleotide phosphate.

genes associated with muscle fibers, such as *flnc* and *myh13*, were significantly up-regulated in YM snakehead. *Flnc* maintains the structural integrity of sarcomeres in striated muscle (Verdonschot et al., 2020), while *myh13* is involved in ATPase activity, crucial for muscle contraction (Weiss & Leinwand, 1996). The differential expression of *myh13* may correlate with variations in energy metabolic pathways, including oxidative phosphorylation, and has been linked to meat quality traits in different pig breeds (Li et al., 2016). The expression of *flnc* is specific to striated muscle and is crucial for maintaining sarcomere structural integrity (Verdonschot et al., 2020), and its dysfunction can lead to myofibrillar rupture (e.g., myofibrillar myopathy) and significantly reduce muscle stiffness and elasticity (Fürst et al., 2013). The contractile properties of muscle fibers, largely determined by myosin heavy chain (MYHC), depend on ATPase activity for energy during muscle contraction; *myh13* encodes one of the MYHCs in skeletal muscle (Weiss & Leinwand, 1996). The differential expression of *myh13* may relate to variations in energy metabolic pathways, such as oxidative phosphorylation, and has been linked to meat quality traits in different pig breeds (Li et al., 2016). Additionally, small heat shock proteins (sHSPs) genes (*hspb8*, *hspb9*, *hspb11*) were also up-regulated in YM snakehead, contributing to muscle sarcomere assembly stability and significantly reduces the accumulation of lipid peroxides, thereby prolonging shelf-life (Marvin et al., 2008). These DEGs provide insights into the muscle texture differences between the two snakeheads.

The KEGG enrichment analysis highlighted the ribosome pathways, where ribosomal proteins were down-regulated. Ribosomes are essential for translation, and studies indicate that ribosome biogenesis regulates protein synthesis and muscle mass in response to contraction and metabolism (Chaillou et al., 2014). Metabolomics results indicated that the composition and metabolism of amino acids, nucleotides, and fatty

acids differed between YM and WT snakehead muscles. We identified DEGs related to lipid metabolism (e.g., *pnpla7*, *lipe*), amino acid metabolism (e.g., *glul*, *ckba*, *tyrp1*) and nucleotide metabolism (e.g., *rrm1*, *pde4b*, *adss2*). In summary, transcriptomic analysis offers insights into the molecular mechanisms underlying the differences in flesh quality between YM and WT snakeheads, highlighting the need for further integrative analysis of transcriptomic and metabolomic data.

4.4. Integrated analysis of transcriptomics and metabolomics

Building upon the individual omics analyses, we performed an integrative analysis to elucidate the regulatory pathways linking genes and metabolites. This analysis highlighted lipid metabolism as a major contributor to nutritional value and flavor differences. Lipid metabolism significantly impacts fish flesh quality. We identified "Glycerophospholipid metabolism" and "Regulation of lipolysis in adipocytes" as key pathways related to lipid metabolism differences. Fatty acids generated in these pathways likely contribute to variations in fatty acid composition. Phospholipids notably influence flavor compounds in meat; their oxidative degradation can produce fishy odor compounds (Frank et al., 2017). Significant differences in phospholipid expression and metabolism were observed between the two snakeheads, leading to a pronounced fishy odor in WT snakehead.

In metabolomics analysis, "Glycerophospholipid metabolism" emerged as the most significant metabolic pathway. Acetylcholine, choline, and glycerophosphocholine were annotated in this pathway and exhibited significantly higher expression in WT snakehead muscle. Additionally, this pathway was notable in the joint-pathway enrichment analysis, suggesting its role as a key regulatory pathway in lipid metabolism. Several glycerophospholipids, including phosphatidylcholine (PC), lysophosphatidylcholine (LysoPC), phosphatidylethanolamine (PE), phosphatidylserine (PS), and phosphatidylinositol (PI), also contributed to the differences between YM and WT snakehead muscle. Most of these metabolites serve as intermediates in the CDP–choline cycle, which is linked to lipid movement in membranes and overall lipid metabolism (Fagone & Jackowski, 2013). PC plays essential physiological roles, being a principal component of cellular membranes, a crucial element of lipoproteins, and a surfactant (Cole et al., 2012). As choline is primarily derived from the diet, we speculate that the elevated expression of these metabolites in WT snakehead may be associated with more active hydrolysis of PC. Gene expression analysis revealed that *pnpla7* and *gpat3* were DEGs in this pathway, both up-regulated in YM snakehead. Research indicates that *pnpla7* has strong hydrolytic activity on LPC, particularly LPC with PUFAs, releasing fatty acids and glycerophosphocholine (Heier et al., 2017). Moreover, *pnpla6*, another highly expressed gene that differed significantly between the two snakeheads, encodes neuropathy target esterase (NTE), which can hydrolyze PC directly to glycerophosphocholine (Zhu et al., 2016). We found strong positive correlations between pnpla6 and several important metabolites.

Furthermore, "Regulation of lipolysis in adipocytes" relates to fat mobilization, encompassing one DM (DG(18:0/20:4(5Z,8Z,11Z,14Z)/0:0)[iso2]) and two DEGs (*prkg2*, *lipe*). DG(18:0/20:4(5Z,8Z,11Z,14Z)/0:0)[iso2] is a diacylglycerol and intermediate in triglyceride catabolism, also serving as a secondary messenger in signal transduction (Berridge, 1984). The genes *prkg2* and *lipe* play roles in catalyzing the hydrolysis of diacylglycerol, highlighting this process as a key pathway contributing to the differences in lipid metabolism.

4.5. Mechanisms underlying muscle color differences

Given the pronounced difference in muscle color between the two snakehead strains, we further investigated the potential molecular mechanisms involved in pigmentation. Muscle color is influenced by both pigment content and redox regulation, which are in turn affected by metabolites and gene expression. Muscle color primarily depends on the quantity and composition of myoglobin, which exists in three main derivatives: deoxymyoglobin, oxymyoglobin, and metmyoglobin. In red muscle species, such as beef (*Bos taurus*), pig (*Sus scrofa*), and bluefin tuna (*Thunnus orientalis*), the slaughtered muscle initially contains high levels of oxymyoglobin, giving it a bright red appearance. Over time, exposure to oxygen causes both deoxymyoglobin and oxymyoglobin to oxidize into metmyoglobin, resulting in the muscle color gradually turning brown (Suman & Joseph, 2013). In this study, the relative content of metmyoglobin was significantly higher in YM snakehead muscle. Since snakehead primarily consists of white muscle, we hypothesize that metmyoglobin may have a different effect on muscle color in this species.

In the metabolomics analysis, "Nicotinate and nicotinamide metabolism" emerged as a key pathway associated with muscle color, encompassing two DMs (nicotinamide and trigonelline). This pathway has been shown to significantly influence meat color in other studies (Fang et al., 2022; Zhan et al., 2022). Nicotinate and nicotinamide synthesize NAD^+ and $NADP^+$ through the Preiss-Handler and salvage pathways, while trigonelline is synthesized by the methylation of nicotinic acid in plants (Ashihara et al., 2015). Trigonelline and its synthesizing enzyme have also been detected in several marine species (Nishitani et al., 1995), though its biosynthetic pathway remains unclear. In this study, nicotinamide expression was significantly lower, while trigonelline expression was significantly higher in YM snakehead muscle. We hypothesize that differences in this pathway contributed to variations in NADH and NADPH levels between YM and WT snakeheads. NADH and NADPH are closely linked to biological redox reactions, such as energy metabolism. The DEGs related to redox processes included those in the "Oxidative phosphorylation" (*atp5f1e*, *myh13*, *ndufb3*, *uqcrq*, *mt-nd5*), "Peroxisome" (*sod1*, *prdx5*), and "Glutathione metabolism" (*gpx1*, *gpx8*, *gstt2b*, *rrm1*, *ggt7*) pathways, with most being downregulated in YM snakehead. We observed strong correlations between genes involved in "Oxidative phosphorylation" and "Peroxisome" and metabolites in "Nicotinate and nicotinamide metabolism". Previous studies have shown that these pathways can influence the redox state of myoglobin, affecting metmyoglobin content and thus muscle color (Bekhit & Faustman, 2005; Wu et al., 2016). Meanwhile, Nicotinamide has been shown to affect skin color by reducing melanosome transfer, and it may influence muscle color through a similar mechanism (Antl et al., 2006). Additionally, glutathione, an important metabolite identified in this study, has been closely linked to meat color due to its antioxidant effect on oxymyoglobin (Tang et al., 2003).

4.6. Implications for breeding and future research

Taken together, the integrative analysis of transcriptomic and metabolomic data provided an effective means to evaluate the flesh quality of snakeheads, encompassing nutrition, taste, flavor, texture, and color. The findings of this study provide important implications for selective breeding strategies in snakehead. The significantly higher content of DHA and lower levels of fishy-flavor VOCs in YM snakehead indicate that this phenotype possesses superior nutritional and sensory qualities, which are highly desirable traits for consumer markets. In addition, the up-regulation of genes associated with muscle fiber structure and antioxidant protection suggests that YM individuals may have improved muscle texture and shelf-life stability. These traits can be used as phenotypic or molecular selection targets in breeding programs to develop high-quality strains with enhanced flesh characteristics.

Compared with previous studies on flesh quality in teleosts, including grass carp (Zhao, Chong, et al., 2018) and Nile tilapia (*Oreochromis niloticus*) (Li et al., 2018), our study integrates both transcriptomic and metabolomic data to reveal a more comprehensive picture of the molecular basis underlying flesh quality traits. While prior studies have typically focused on either lipid content or specific flavor compounds, our integrative analysis identifies key regulatory pathways—such as "Glycerophospholipid metabolism" and "Nicotinate and nicotinamide metabolism"—that are directly associated with lipid

mobilization, redox state, and muscle color. These insights demonstrate the novelty of our study in elucidating multi-layered molecular interactions that contribute to phenotype variation. This study is the first to use a multi-omics approach to elucidate the molecular mechanisms underlying flesh quality differences between the wild-type and a body color mutant strain in an economically important aquaculture fish species. Importantly, the identified differentially expressed metabolites and genes may serve as biomarkers for snakehead flesh quality and could be applied to develop rapid selection or screening tools in breeding practices. The use of metabolomic and transcriptomic markers represents a forward-looking approach that could enhance the efficiency and precision of aquaculture breeding programs.

5. Conclusions

This study conducted a comprehensive comparison of flesh quality between YM and WT snakeheads, by integrating phenotypic assessment, metabolomic profiling, and transcriptomic analysis. Compared to WT snakehead, YM snakehead exhibited redder muscle color, improved nutritional value (e.g., higher DHA), and a milder fishy odor, indicating superior flesh quality. Through integrated multi-omics analysis, we found that DEGs (e.g., *pnpla7*, *lipe*, and *prkg2*) may regulate differences in lipid metabolism between YM and WT snakeheads by modulating DMs (acetylcholine, choline, and glycerophosphocholine) in the "Glycerophospholipid metabolism" pathway, thereby contributing to differences in nutritional value and flavor. In terms of muscle color, DMs (nicotinamide, trigonelline, and glutathione) and DEGs (e.g., *atp5f1e*, *myh13*, *ndufb3*, and *mt-nd5*) may influence the redox state of myoglobin by participating in oxidative-reduction processes, affecting the accumulation of metmyoglobin and ultimately leading to color variation between the two strains. These findings not only provide scientific evidence supporting the superior flesh quality of YM snakehead over the wild-type, but also deepen our biological understanding of phenotypic variation between the two strains. Moreover, the results offer a theoretical foundation for the development of high-quality snakehead strains in aquaculture.

CRediT authorship contribution statement

Donglei Sun: Writing – review & editing, Writing – original draft, Visualization, Validation, Investigation. **Zexin Tao:** Visualization, Validation, Methodology, Investigation, Formal analysis. **Haishen Wen:** Methodology, Investigation, Formal analysis. **Xin Qi:** Validation, Methodology, Investigation. **Chao Li:** Resources, Funding acquisition. **Lingyu Wang:** Visualization, Validation, Investigation. **Xiaoyan Zhang:** Validation, Methodology, Investigation. **Yun Li:** Supervision, Resources, Project administration, Conceptualization.

Declaration of competing interest

The authors declare that they have no known competing financial interests or personal relationships that could have appeared to influence the work reported in this paper.

Acknowledgments

This work was supported by Shandong Technical System of Fish Industry (SDAIT-12-03). We acknowledge the support of the High-Performance Biological Supercomputing Center at the Ocean University of China for this research.

Appendix A. Supplementary data

Supplementary data to this article can be found online at https://doi.org/10.1016/j.fbio.2025.106496.

Data availability

Data will be made available on request.

References

Antl, M., von Brühl, M.-L., Eiglsperger, C., Werner, M., Konrad, I., Kocher, T., Wilm, M., Hofmann, F., Massberg, S., & Schlossmann, J. (2006). IRAG mediates NO/cGMP-dependent inhibition of platelet aggregation and thrombus formation. *Blood, 109*(2), 552–559. https://doi.org/10.1182/blood-2005-10-026294

Ashihara, H., Ludwig, I. A., Katahira, R., Yokota, T., Fujimura, T., & Crozier, A. (2015). Trigonelline and related nicotinic acid metabolites: Occurrence, biosynthesis, taxonomic considerations, and their roles in planta and in human health. *Phytochemistry Reviews, 14*(5), 765–798. https://doi.org/10.1007/s11101-014-9375-z

Astarita, G., Ahmed, F., & Piomelli, D. (2008). Identification of biosynthetic precursors for the endocannabinoid anandamide in the rat brain. *Journal of Lipid Research, 49*(1), 48–57. https://doi.org/10.1194/jlr.m700354-jlr200

Beg, M. M., Roy, S. M., Moulick, S., & Mandal, B. (2023). Quality evaluation of organically farmed fish fillet of Indian major carps. *Aquaculture International, 31*(5), 2743–2761. https://doi.org/10.1007/s10499-023-01107-6

Bekhit, A. E. D., & Faustman, C. (2005). Metmyoglobin reducing activity. *Meat Science, 71*(3), 407–439. https://doi.org/10.1016/j.meatsci.2005.04.032

Berridge, M. J. (1984). Inositol trisphosphate and diacylglycerol as second messengers. *Biochemical Journal, 220*(2), 345–360.

Beyoğlu, D., & Idle, J. R. (2013). Metabolomics and its potential in drug development. *Biochemical Pharmacology, 85*(1), 12–20. https://doi.org/10.1016/j.bcp.2012.08.013

Bodin, N., Amiel, A., Fouché, E., Sardenne, F., Chassot, E., Debrauwer, L., Guillou, H., Tremblay-Franco, M., & Canlet, C. (2022). NMR-based metabolic profiling and discrimination of wild tropical tunas by species, size category, geographic origin, and on-board storage condition. *Food Chemistry, 371*, Article 131094. https://doi.org/10.1016/j.foodchem.2021.131094

Calvani, M., Reda, E., & Arrigoni-Martelli, E. (2000). Regulation by carnitine of myocardial fatty acid and carbohydrate metabolism under normal and pathological conditions. *Basic Research in Cardiology, 95*(2), 75–83. https://doi.org/10.1007/s003950050167

Chaillou, T., Kirby, T. J., & McCarthy, J. J. (2014). Ribosome biogenesis: Emerging evidence for a central role in the regulation of skeletal muscle mass. *Journal of Cellular Physiology, 229*(11), 1584–1594. https://doi.org/10.1002/jcp.24604

Cole, L. K., Vance, J. E., & Vance, D. E. (2012). Phosphatidylcholine biosynthesis and lipoprotein metabolism. *Biochimica et Biophysica Acta (BBA) - Molecular and Cell Biology of Lipids, 1821*(5), 754–761. https://doi.org/10.1016/j.bbalip.2011.09.009

Fagone, P., & Jackowski, S. (2013). Phosphatidylcholine and the CDP–choline cycle. *Biochimica et Biophysica Acta (BBA) - Molecular and Cell Biology of Lipids, 1831*(3), 523–532. https://doi.org/10.1016/j.bbalip.2012.09.009

Fang, J., Feng, L., Lu, H., & Zhu, J. (2022). Metabolomics reveals spoilage characteristics and interaction of Pseudomonas lundensis and Brochothrix thermosphacta in refrigerated beef. *Food Research International, 156*, Article 111139. https://doi.org/10.1016/j.foodres.2022.111139

Fauconneau, B., Alami-Durante, H., Laroche, M., Marcel, J., & Vallot, D. (1995). Growth and meat quality relations in carp. *Aquaculture, 129*(1), 265–297. https://doi.org/10.1016/0044-8486(94)00309-C

Fiehn, O. (2002). Metabolomics—the link between genotypes and phenotypes. *Plant Molecular Biology, 48*(1–2), 155–171.

Frank, D., Kaczmarska, K., Paterson, J., Piyasiri, U., & Warner, R. (2017). Effect of marbling on volatile generation, oral breakdown and in mouth flavor release of grilled beef. *Meat Science, 133*, 61–68. https://doi.org/10.1016/j.meatsci.2017.06.006

Fürst, D. O., Goldfarb, L. G., Kley, R. A., Vorgerd, M., Olivé, M., & van der Ven, P. F. (2013). Filamin C-related myopathies: Pathology and mechanisms. *Acta Neuropathologica, 125*, 33–46. https://doi.org/10.1093/hmg/ddw135

Gjedrem, T. (1997). Flesh quality improvement in fish through breeding. *Aquaculture International, 5*(3), 197–206. https://doi.org/10.1023/A:1014546816984

Hayat, M., Khan, B., Iqbal, J., Ahmad, M. N., Khan, A. A., Haq, T. U., … Albekairi, T. H. (2024). Evidence of microplastic contamination in the food chain: An assessment of their presence in the gastrointestinal tract of native fish. *Italian Journal of Food Science, 36*(3), 40. https://doi.org/10.15586/ijfs.v36i3.2532

Heier, C., Kien, B., Huang, F., Eichmann, T. O., Xie, H., Zechner, R., & Chang, P.-A. (2017). The phospholipase PNPLA7 functions as a lysophosphatidylcholine hydrolase and interacts with lipid droplets through its catalytic domain. *Journal of Biological Chemistry, 292*(46), 19087–19098. https://doi.org/10.1074/jbc.M117.792978

Horrocks, L. A., & Yeo, Y. K. (1999). Health benefits of docosahexaenoic acid (DHA). *Pharmacological Research, 40*(3), 211–225. https://doi.org/10.1006/phrs.1999.0495

Kawai, M., Okiyama, A., & Ueda, Y. (2002). Taste enhancements between various amino acids and IMP. *Chemical Senses, 27*(8), 739–745. https://doi.org/10.1093/chemse/27.8.739

Khan, B. N., Ashfaq, Y., Hussain, N., Atique, U., Aziz, T., Alharbi, M., … Alasmari, A. F. (2023). Elucidating the effects of heavy metals contamination on vital organ of fish and migratory birds found at fresh water ecosystem. *Heliyon, 9*(11), Article e20968. https://doi.org/10.1016/j.heliyon.2023.e20968

Krzywicki, K. (1982). The determination of haem pigments in meat. *Meat Science, 7*(1), 29–36. https://doi.org/10.1016/0309-1740(82)90095-X

Kuchiba-Manabe, M., Matoba, T., & Hasegawa, K. (1991). Sensory changes in umami taste of inosine 5′-monophosphate solution after heating. *Journal of Food Science, 56* (5), 1429–1432. https://doi.org/10.1111/j.1365-2621.1991.tb04790.x

Li, M., Wang, X., Qi, C., Li, E., Du, Z., Qin, J. G., & Chen, L. (2018). Metabolic response of Nile tilapia (*Oreochromis niloticus*) to acute and chronic hypoxia stress. *Aquaculture, 495*, 187–195. https://doi.org/10.1016/j.aquaculture.2018.05.031

Li, X. J., Zhou, J., Liu, L. Q., Qian, K., & Wang, C. L. (2016). Identification of genes in longissimus dorsi muscle differentially expressed between Wannanhua and Yorkshire pigs using RNA-sequencing. *Animal Genetics, 47*(3), 324–333. https://doi.org/10.1111/age.12421

Ling, L., Liu, Y., Zhang, X., Aziz, T., Shahzad, M., Sameeh, M. Y., … Zhu, Y. (2023). Effect of *Flammulina velutipes* polysaccharides on the physicochemical properties of catfish surimi and myofibrillar protein oxidation during frozen storage. *Frontiers in Nutrition, 10*, Article 1268580. https://doi.org/10.3389/fnut.2023.1268580

Liu, Y., Huang, Y., Wang, Z., Cai, S., Zhu, B., & Dong, X. (2021). Recent advances in fishy odour in aquatic fish products, from formation to control. *International Journal of Food Science and Technology, 56*(10), 4959–4969. https://doi.org/10.1111/ijfs.15269

Lv, H. B., Ma, Y., Hu, C. T., Lin, Q. Y., Yue, J., Chen, L. Q., Zhang, M. L., Du, Z. Y., & Qiao, F. (2021). The individual and combined effects of hypoxia and high-fat diet feeding on nutrient composition and flesh quality in Nile tilapia (*Oreochromis niloticus*). *Food Chemistry, 343*, Article 128479. https://doi.org/10.1016/j.foodchem.2020.128479

Marvin, M., O'Rourke, D., Kurihara, T., Juliano, C. E., Harrison, K. L., & Hutson, L. D. (2008). Developmental expression patterns of the zebrafish small heat shock proteins. *Developmental Dynamics, 237*(2), 454–463. https://doi.org/10.1002/dvdy.21414

Meléndez-Hevia, E., de Paz-Lugo, P., Cornish-Bowden, A., & Cárdenas, M. L. (2009). A weak link in metabolism: The metabolic capacity for glycine biosynthesis does not satisfy the need for collagen synthesis. *Journal of Biosciences, 34*(6), 853–872. https://doi.org/10.1007/s12038-009-0100-9

Nishitani, H., Kikuchi, S., Okumura, K., & Taguchi, H. (1995). Finding of a homarine-synthesizing enzyme in turban shell and some properties of the enzyme. *Archives of Biochemistry and Biophysics, 322*(2), 327–332. https://doi.org/10.1006/abbi.1995.1471

Suman, S. P., & Joseph, P. (2013). Myoglobin chemistry and meat color. *Annual Review of Food Science and Technology, 4*(1), 79–99. https://doi.org/10.1146/annurev-food-030212-182623

Sun, D., Qi, X., Wen, H., Li, C., Li, J., Chen, J., Tao, Z., Zhu, M., Zhang, X., & Li, Y. (2023). The genetic basis and potential molecular mechanism of yellow-albino northern snakehead (*Channa argus*). *Open biology, 13*(2), Article 220235. https://doi.org/10.1098/rsob.220235

Tang, J., Faustman, C., Lee, S., & Hoagland, T. A. (2003). Effect of glutathione on oxymyoglobin oxidation. *Journal of Agricultural and Food Chemistry, 51*(6), 1691–1695. https://doi.org/10.1021/jf025924f

Verdonschot, J. A. J., Vanhoutte, E. K., Claes, G. R. F., Helderman-van den Enden, A. T. J. M., Hoeijmakers, J. G. J., Hellebrekers, D. M. E. I., de Haan, A., Christiaans, I., Lekanne Deprez, R. H., Boen, H. M., van Craenenbroeck, E. M., Loeys, B. L., Hoedemaekers, Y. M., Marcelis, C., Kempers, M., Brusse, E., van Waning, J. I., Baas, A. F., Dooijes, D., … Brunner, H. G. (2020). A mutation update for the FLNC gene in myopathies and cardiomyopathies. *Human Mutation, 41*(6), 1091–1111. https://doi.org/10.1002/humu.24004

Wang, J., & Yang, G. (2011). The complete mitogenome of the snakehead *Channa argus* (Perciformes: Channoidei): Genome characterization and phylogenetic implications. *Mitochondrial DNA, 22*(4), 120–129. https://doi.org/10.3109/19401736.2011.624599

Weiss, A., & Leinwand, L. A. (1996). The mammalian myosin heavy chain gene family. *Annual Review of Cell and Developmental Biology, 12*, 417–439. https://doi.org/10.1146/annurev.cellbio.12.1.417

Wu, W., Yu, Q. Q., Fu, Y., Tian, X. J., Jia, F., Li, X. M., & Dai, R. T. (2016). Towards muscle-specific meat color stability of Chinese luxi yellow cattle: A proteomic insight into post-mortem storage. *Journal of Proteomics, 147*, 108–118. https://doi.org/10.1016/j.jprot.2015.10.027

Xiao, M., Qian, K., Wang, Y., & Bao, F. (2020). GC-MS metabolomics reveals metabolic differences of the farmed Mandarin fish Siniperca chuatsi in recirculating ponds aquaculture system and pond. *Scientific Reports, 10*(1), 1–8. https://doi.org/10.1038/s41598-020-63252-9

Young, T., & Alfaro, A. (2018). Showcasing metabolomic applications in aquaculture: A review. *Reviews in Aquaculture, 10*, 135–152. https://doi.org/10.1111/raq.12152

Yu, H., Zhang, R., Yang, F., Xie, Y., Guo, Y., Yao, W., & Zhou, W. (2021). Control strategies of pyrazines generation from Maillard reaction. *Trends in Food Science & Technology, 112*, 795–807. https://doi.org/10.1016/j.tifs.2021.04.028

Yu, H., Zou, Z. X., Wei, W., & Li, Y. (2024). Conjugated linoleic acid reduces lipid accumulation via down-regulation expression of lipogenic genes and up-regulation of apoptotic genes in grass carp (*Ctenopharyngodon idella*) adipocyte in vitro. *Marine Biotechnology, 26*(1), 169–180. https://doi.org/10.1007/s10126-024-10286-z

Zhan, H., Xiong, Y., Wang, Z., Dong, W., Zhou, Q., Xie, S., Li, X., Zhao, S., & Ma, Y. (2022). Integrative analysis of transcriptomic and metabolomic profiles reveal the complex molecular regulatory network of meat quality in Enshi black pigs. *Meat Science, 183*, Article 108642. https://doi.org/10.1016/j.meatsci.2021.108642

Zhao, H., Chong, J., Tang, R., Li, L., Xia, J., & Li, D. (2018a). Metabolomics investigation of dietary effects on flesh quality in grass carp (*Ctenopharyngodon idellus*). *GigaScience, 7*(10). https://doi.org/10.1093/gigascience/giy111

Zhao, H., Xia, J., Zhang, X., He, X., Li, L., Tang, R., Chi, W., & Li, D. (2018b). Diet affects muscle quality and growth traits of grass carp (*Ctenopharyngodon idellus*): A comparison between grass and artificial feed. *Frontiers in Physiology, 9*, 283. https://doi.org/10.3389/fphys.2018.00283

Zhou, B., Xiao, J. F., Tuli, L., & Ressom, H. W. (2012). LC-MS-based metabolomics. *Molecular BioSystems, 8*(2), 470–481. https://doi.org/10.1039/C1MB05350G

Zhu, X., Hao, R., Tian, C., Zhang, J., Zhu, C., & Li, G. (2021). Integrative transcriptomics and metabolomics analysis of body color formation in the leopard coral grouper (*Plectropomus leopardus*). *Frontiers in Marine Science, 8*, Article 726102. https://doi.org/10.3389/fmars.2021.726102

Zhu, L., Wang, P., Sun, Y. J., Xu, M. Y., & Wu, Y. J. (2016). Disturbed phospholipid homeostasis in endoplasmic reticulum initiates tri-o-cresyl phosphate-induced delayed neurotoxicity. *Scientific Reports, 6*(1), 1. https://doi.org/10.1038/srep37574

Zuo, R., Ai, Q., Mai, K., Xu, W., Wang, J., Xu, H., Liufu, Z., & Zhang, Y. (2012). Effects of dietary n-3 highly unsaturated fatty acids on growth, nonspecific immunity, expression of some immune related genes and disease resistance of large yellow croaker (*Larmichthys crocea*) following natural infestation of parasites (*Cryptocaryon irritans*). *Fish & Shellfish Immunology, 32*(2), 249–258. https://doi.org/10.1016/j.fsi.2011.11.005